Effects of Solvent Polarity on Li-ion Diffusion in Polymer Electrolytes: An All-Atom Molecular Dynamics Study with Charge Scaling

Harish Gudla, Chao Zhang,* and Daniel Brandell

ACCESS | Metrics & More | Article Recommendations | Supporting Information

ABSTRACT: We herein report an all-atom molecular dynamics study on the role of solvent polarity for Li^+ diffusion in polymer electrolytes using PEO−LiTFSI (poly(ethylene oxide)−lithium bis(trifluoromethane)sulfonimide) as a model system. By separating the effect of T_g and the effect of solvent polarity in our simulations, we show that the maximum in the diffusion coefficient of Li^+ with respect to the dielectric constant of polymer solvent ε_p is due to transitions in the transport mechanism. In particular, it is found that the frequent interchain hopping involves the coordination of both PEO and TFSI. This optimal solvating ability of PEO at an intermediate value of ε_p leads to the fast ion conduction. These findings highlight the synergetic effect of solvent polarity and bond polarity on Li-ion diffusion in solid polymer electrolytes.
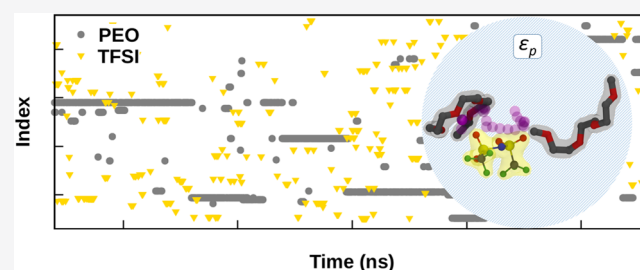
1. INTRODUCTION

Solid (solvent-free) polymer electrolytes (SPEs) are promising alternatives to conventional liquid counterparts, which enhance the safety, the flexibility, and the reduction of the leakage in Li-ion batteries.[1,2] However, one of the remaining yet decisive bottlenecks in the development of polymer electrolytes is the limited ionic conductivity at room temperature. The ionic conductivity in polymer electrolytes depends on a variety of factors such as polymer structure, molecular weight, glass transition temperature (T_g), end/side-chain groups, salt concentration, donor number, solvent polarity, etc.[3−10] To understand the coupling between these factors, to disentangle their contributions to the ion transportation, and to use this knowledge for designing new types of SPEs, constitute the grand challenges in the field. To this end, modeling by computer simulations can provide significant aid since these aspects can be studied systematically.

Factors such as solvent polarity, T_g and donor number control the solvating ability of salt in the polymer systems and thus directly affect the conductivity of ions.[11−14] However, these factors are highly coupled, rendering it difficult to determine the influence of these parameters on ionic mobility and have been little explored for polymer electrolyte systems. In a recent experimental study on the ion conduction in poly(glycidyl ether)-based lithium bis(trifluoromethyl)-sulfonimide (LiTFSI) electrolytes,[15] it was found that the measured ionic conductivity (but not cation and anion diffusivities) increases monotonically with the host polymer dielectric constant. This triggered a full atomistic molecular dynamics (MD) simulations study on these electrolytes.[16] The

simulations could qualitatively reproduce the experimental trends and attributed the observed increase in ionic conductivity in the polymer matrix of high solvent polarity to an ameliorated ion aggregation and more free charge carriers. To further investigate the dependence of polymer polarity on ionic conduction, this study was followed by coarse-grained simulations using a Stockmayer model for neat and salt (LiTFSI) doped poly(ethylene oxide) (PEO) electrolytes.[17] Therein, the point dipole moment of the EO monomer was scaled as an indicator of the solvent polarity strength. It was found that the ionic conductivity, as well as diffusivities from the Nernst−Einstein relation, reaches a maximum at an intermediate dipole strength. This optimal point was rationalized as a trade-off between ionic aggregation and polymer segmental dynamics, i.e., a further increased polarity reduces the polymer segmental motion due to enhanced polymer−polymer interactions and thereby reduces ion transport. However, the polarity of polymer electrolytes involves both the dielectric effect of the solvent and the bond polarity resulting from the local effect of coordination and quantified by the donor number.[18] Moreover, the effect that the increased polymer dielectric constant leads to enhanced ionic conductivity may be solely attributed to the shift in T_g, as

shown in experiments by tuning the backbone polarity.[19] Therefore, a fully atomistic picture beyond coarse-grained models for disentangling these factors is needed.

In all-atom simulations, many-body polarizable force field[20,21] can provide accurate results for electrolytes with Li salts through either the atomic polarizability model or the fluctuating charge model. However, these methods are limited by high computational cost for long time-scale simulations. Instead, scaling the point charges in force fields is an effective approach to introduce electronic polarizations where the point charges of salt ions are scaled down to screen the polymer−ion and ion−ion interactions. The charge scaling factor (f) of salt ions is related to the optical dielectric constant of the solvent (ϵ_∞) by refs.[22−25] In simulations of polymer electrolytes, a scaling factor between 0.5 and 0.8 has been commonly used for salt ions in recent years,[26−29] which has shown to better reproduce experimental diffusivities. A less used approach in MD studies of SPEs is to scale the point charge of solvent molecules to modulate the solvent polarity. A well-known example of this type is the rigid three-point water model, which employs an enhanced dipole moment of 2.35 D for liquid water simulations instead of the gas phase value of 1.85 D.[30] Note that the effect of bond polarity is included implicitly by scaling charges of salt and solvent since the local solvation environment is dominated by the electrostatic interaction.

In this work, we aim to examine the effects of polarity by employing all-atom MD simulations with charge scaling and taking the PEO−LiTFSI system as a prototype. After describing the computational setups, we first show how to use the dielectric constant of polymer solvent ε_p to gauge the strength of solvent polarity and discuss the relation between solvent polarity and the glass transition temperature (T_g). Then, by separating the effect of T_g and the effect of solvent polarity, we show how solvent polarity affects polymer dynamics and ion conduction and leads to an optimal point in terms of the self-diffusion coefficient of Li^{+}. This is followed by a discussion on how local solvation environments (bond polarity) affect the ion-transport mechanisms in polymer electrolyte systems and couples to the solvent polarity. Overall, these point out that the optimal solvating ability of PEO at the intermediate value of ε_p leads to the maximum of D_{Li^+} and balanced interactions between Li ion with TSFI and PEO lead to frequent interchain hopping of Li^{+}.

2. COMPUTATIONAL METHODS

MD simulation boxes comprising neat and LiTFSI-doped PEO systems were constructed, comprising 200 hydroxyl-terminated chains, each with 25 monomer units (1.11 kg/mol) and 400 Li and 400 TFSI ions, corresponding to a [Li^{+}]/[EO] concentration ratio of 0.08. The initial configurations of the simulation boxes were generated through a random arrangement of polymer chains and ions, using PACKMOL package.[31] Then, the total energy of the initial system was minimized using the steepest descent algorithm.

General AMBER force field (GAFF) parameters[32] were used for describing bonding and nonbonding interactions in PEO and LiTFSI.[33−35] The AM1-BCC (bond charge correction)[36] model was used to assign the partial atomic charges (see Section A in the Supporting Information), which emulates the HF/6-31G* electrostatic potential (ESP) of a molecule. The van der Waals parameters used were the same as those implemented in the standard AMBER force field.[32]

All MD simulations were performed using GROMACS 2018.1.[37,38] The long-range electrostatic interactions were employed through a particle mesh Ewald technique[39] with an interpolation order of 4 and a grid size of 0.16 nm. The short-range cutoff distances of the van der Waals and Coulombic interaction in the direct space are 1 nm. The bonds involving hydrogen atoms were constrained using the LINCS algorithm.[40] For all MD simulations, the leapfrog integrator was employed with a time step of 1 fs.

MD simulations in the NVT (constant number, volume, and temperature) and NPT (constant number, pressure, and temperature) ensembles were performed subsequently for the purpose of equilibration using a Bussi−Donadio−Parrinello thermostat[41] and a Parrinello−Rahman barostat[42] at 400 K and 1 bar for 5 and 10 ns, respectively. In the NVT and NPT equilibration runs, the temperature and the density of the system were equilibrated respectively. During these simulations, the coupling constants for the thermostat and the barostat were set to 0.1 ps and 2.0 ps, respectively. Appropriate polymer equilibration was confirmed by comparing the mean squared displacement (MSD) of the PEO chains at the end of simulation and R_g^2 and calculating the polymer end-to-end vector autocorrelations (see Section B in the Supporting Information for details). To determine the T_g of both neat and salt-doped systems, a stepwise NPT cooling from 400 to 140 K with a step of 20 K was performed for 20 ns at each given temperature. The densities of the system at each temperature were calculated from the last 5 ns of the simulation. To investigate the structural and transport properties of the LiTFSI-doped PEO systems, NPT simulations were carried out for 300 to 600 ns at different temperatures.

In Table 1, each system is labeled according to the scaling factor f on the point charges in a polymer (P) and salt (S). For example, in the system $P_{1.50}S_{0.75}$, the charges on polymer and salt are scaled by factors of 1.50 and 0.75 respectively.

Table 1. System Notations for Different Charge Scaling Schemes on Polymer and Salt with Simulation Time and Box Size after Equilibrations and Calculated T_g

system notation	charge scaling factor of PEO	charge scaling factor of salt	simulation time (ns)	box size (nm³)	T_g (K)
PEO−LiTFSI					
$P_{1.50}S_{1.00}$	1.50	1.00	600	430	317 (4)
$P_{1.20}S_{1.00}$	1.20		400	437	308 (2)
$P_{1.00}S_{1.00}$	1.00		400	444	304 (4)
$P_{0.75}S_{1.00}$	0.75		550	452	295 (4)
$P_{0.50}S_{1.00}$	0.50		550	460	283 (3)
$P_{1.50}S_{0.75}$	1.50	0.75	300	441	310 (4)
$P_{1.33}S_{0.75}$	1.34		300	443	304 (4)
$P_{1.20}S_{0.75}$	1.20		300	447	299 (4)
$P_{1.00}S_{0.75}$	1.00		300	450	294 (5)
$P_{0.75}S_{0.75}$	0.75		300	454	284 (4)
$P_{0.56}S_{0.75}$	0.56		300	457	277 (2)
$P_{0.45}S_{0.75}$	0.45		300	460	269 (3)
Neat PEO					
$P_{1.50}$	1.50		50	325	302 (3)
$P_{1.00}$	1.00		50	347	286 (2)
$P_{0.75}$	0.75		50	351	280 (3)
$P_{0.50}$	0.50		50	359	272 (2)

3. RESULTS AND DISCUSSION

3.1. Relation between Solvent Polarity and Glass Transition Temperature. The dielectric constant of the polymer electrolyte ε_p reflects the strength of solvent polarity.[43] Since the MD simulations here were performed with periodic boundary conditions and Ewald summation, the dielectric constant of neat and salt-doped PEO can be computed from the fluctuations in the total dipole moment $\mathbf{M}$ of the PEO via the equation for a nonpolarizable model[44]

$$\varepsilon_p = 1 + \frac{4\pi}{3\varepsilon_0 V k_B T}(\langle \mathbf{M}^2 \rangle - \langle \mathbf{M} \rangle^2) \tag{1}$$

where ε_0 is the vacuum permittivity, k_B is Boltzmann's constant, T is the temperature, V is the average volume of the simulation box, and $\langle \ \rangle$ is the ensemble averages. In experimental studies, the dielectric constant can mainly be tuned by changing the polymer chemistry through side chains[15,16] or backbone.[19] For the same polymer electrolyte, it can, for example, be varied also by changing the salt concentration and temperature, and then their relations to the ionic conductivity can be observed.[45,46]

The calculated ε_p value for neat PEO at $P_{1.00}$ in Figure 1a is in good agreement with the reported experimental values in
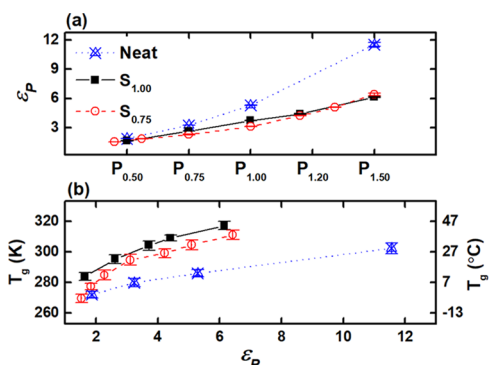

Figure 1. (a) Dielectric constants of PEO (ε_p) in the neat and salt-doped systems at different charge scaling schemes (see Table 1). (b) T_g of neat and salt-doped polymers as a function of the solvent polarity ε_p.

the literature ($\varepsilon \sim 4-5$).[16,47−49] Adding salt to the PEO matrix reduces the dielectric constant as the reorientation of the solvent is significantly hindered. From Figure 1a, one can see that the solvent polarity of a system was enhanced by scaling up the charge on the polymer. This dependence was expected, as the dipole moment is proportional to the atomic charge. The scaling of point charges of slat ions in the $S_{0.75}$ case will introduce an electronic screening in polymer−ion and ion−ion interactions. Interestingly, when comparing the results of $S_{1.00}$ and $S_{0.75}$ cases, it was found that the introduction of electronic polarization has a limited effect on the values of ε_p. This confirms that the electronic polarization can be singled out by scaling charges of PEO and LiTFSI salt separately.

Before discussing the dependence of the glass transition temperature T_g on the solvent polarity, it is worth pointing out that the calculated T_g of $P_{1.00}S_{1.00}$ is 304(4) K (Table 1; also see Section C in the Supporting Information for details), which is about 75 K above the experimentally observed value of 230 K[4,50] for the system with similar molecular weight (M_w = 1.05 kg/mol) and salt concentration (0.05−0.1). This is commonly seen in MD simulations of SPEs due to limitations in the force

field parameters.[51] Because of this noticeable difference in the T_g between experimental and simulated systems, the normalized temperatures ($T - T_0$) should be used. Here, T_0 is taken as 50 K below the T_g, which was suggested to give the best fit to experimental data.[52,53]

In Figure 1b, we can see that the T_g increases when the solvent polarity ε_p becomes larger. This is due to the increased polymer−polymer interactions that reduce the free volume. A comparison of the neat and LiTFSI-doped systems gives a difference of 10−20 K for all the cases, which is also observed experimentally.[54,55] This originates from the restrictions of the polymer segmental motion with the inclusion of salt, which forms physical cross-links of the polymer chains. Since the electrostatic interactions are weaker between the salt and the polymer chains in the $S_{0.75}$ cases than those in the $S_{1.00}$ cases, this leads to the decrement of T_g in the system for $S_{0.75}$.

3.2. Impact of Solvent Polarity on Li-Ion Conduction and Polymer Dynamics. The self-diffusion coefficient (D) for the ions and the polymer chains were used to probe polymer dynamics and ion mobility. D is calculated from MSD curves using the Einstein relation

$$D = \frac{1}{6t} \sum_{i=1}^{N} \lim_{t \to \infty} \langle \| \mathbf{r}_i(t) - \mathbf{r}_i(0) \|^2 \rangle \tag{2}$$

where $\mathbf{r}_i(t)$ and $\mathbf{r}_i(0)$ are the center of the mass of entity i at times t and 0, respectively.[56] Specifically, the MSD(t) curves for Li$^+$ and TFSI were calculated using the center of mass of the corresponding ions, and those for polymer chains were obtained using the oxygen atoms. The self-diffusion coefficient was calculated using the diffusive regime of the simulation, i.e., MSD(t) $\sim t$ (see Section D in the Supporting Information for details). In most cases, this was achieved after $\sim$150 ns at temperatures above 400 K, while longer simulations (>500 ns) were needed at lower temperatures.

The self-diffusion coefficient of Li$^+$ (D_{Li^+}) as a function of normalized temperature ($1000/(T - T_g + 50)$) is shown in Figure 2. It can be seen that when increasing the solvent
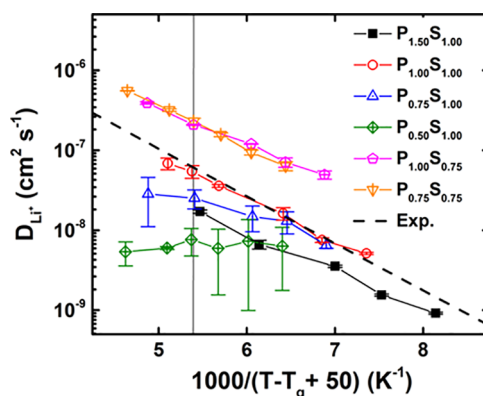

Figure 2. Li$^+$ self-diffusion coefficient (D_{Li^+}) as a function of normalized inverse temperature for different charge scaling schemes. The experimental line was taken from ref 55.

polarity from $P_{0.50} S_{1.00}$ to $P_{1.50} S_{1.00}$, the intercept of D_{Li^+} vs ($1000/(T - T_g + 50)$) becomes smaller as well as the slope of the corresponding curve. This means that Li$^+$ diffusions in these polymer electrolyte systems follow the so-called Meyer−Neldel rule in the low to intermediate range of ε_p, where the prefactor goes down together with the activation energy.[57] An

exception was found for the highest solvent polarity ($P_{1.50}$ $S_{1.00}$), which suggests a different ion-transport mechanism, as will be discussed later.

When compared with the experimental data,[55] the $P_{1.00}S_{1.00}$ system seems to have the best agreement. However, this is fortuitous. Although the experimental PEO–LiTFSI system has the same salt concentration as the simulation system, the corresponding molecular weight is much higher (M_w = 100 kg/mol). In studies of the dependence of molecular weight and chain length of PEO on D_{Li^+}, is has been shown that D_{Li^+} increases by 20−25% when M_w decreases from 100 to 1 kg/mol[5]. This means that $S_{0.75}$, which includes the electronic polarization, might actually constitute a better approximation for use in MD simulations of this system.

To separate the different effects of solvent polarity and T_g, cross-sectional data for D_{Li^+} at a chosen normalized inverse temperature of $1000/(T − T_g + 50) = 5.4 (\pm0.1)$, as indicated by the vertical line in Figure 2, were selected for a range of different polarities. As shown in Figure 3a, for both $S_{1.00}$ and
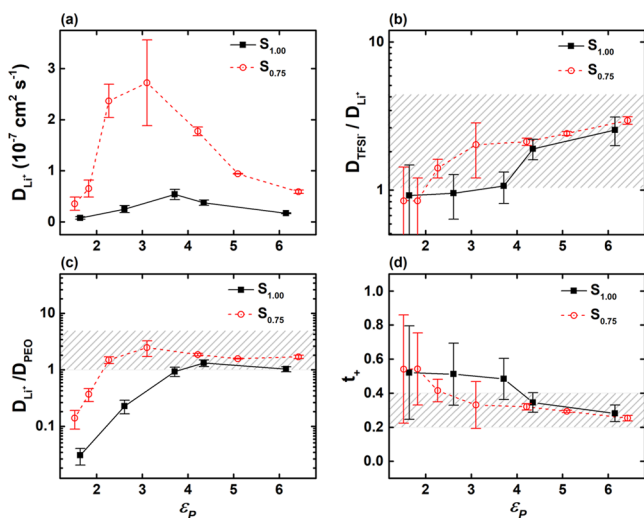

Figure 3. (a) Li$^+$ self-diffusion coefficient (D_{Li^+}), (b) D_{TFSI}/D_{Li^+}, (c) D_{Li^+}/D_{PEO}, and (d) cation transference number (t_+) as a function of solvent polarity at the normalized inverse temperature $1000/(T − T_g + 50)$ of 5.4 (±0.1). Gray region corresponds to the expected values $D_{TFSI}/D_{Li^+} > 1$, $D_{Li^+}/D_{PEO} > 1$ and $t_+ \sim 0.2−0.4$.

$S_{0.75}$ cases, similar trends are found and maxima in $D_{Li^+} (\varepsilon_p)$ appear at $\varepsilon_p = 3−4$. However, the maximum is shifted to lower ε_p and a higher D_{Li^+} is obtained in the case of $S_{0.75}$. These observations will be discussed later by looking at the ion-transport mechanisms and local coordination environments (Sections 3.3 and 3.4).

In the PEO−LiTFSI systems, it is known from experiments that the magnitude of self-diffusion coefficients of each component should follow the order $D_{TFSI} \gg D_{Li^+} > D_{PEO}$ during extended time scales.[58,59] In Figure 3b,c, one can see how the solvent polarity modulates this sequence. It is found that when the value of ε_p is low, $D_{PEO} \gg D_{TFSI} \sim D_{Li^+}$. This suggests that there is significant ion-pairing due to the poor screening from the solvent and that the diffusion of Li$^+$ is decoupled from the polymer matrix. Instead, when ε_p becomes larger, the expected order $D_{TFSI} \gg D_{Li^+} > D_{PEO}$ appears. In this regime, D_{Li^+}/D_{PEO} is larger than 1, which indicates that the lithium-ion transport occurs via a hopping mechanism between different coordinating sites.

In addition, the cation transference number (t_+) was calculated from self-diffusion coefficients of cation and anion as follows

$$t_+ = \frac{D_{Li^+}}{D_{Li^+} + D_{TFSI}} \tag{3}$$

Figure 3d shows the dependence of t_+ on solvent polarity. The t_+ is nearly 0.5 at low ε_p values, which is likely coupled to the formation of ion pairs and that the ionic species migrate together. At high ε_p, on the other hand, the t_+ values are closer to experimentally observed transference numbers; 0.2−0.3 for systems with a similar molecular weight of polymer at the same salt concentration.[4,6,59]

3.3. Impact of Solvent Polarity on Li-Ion Transport Mechanism. As discussed, the effect of solvent polarity on Li-ion mobility is not monotonic. For example, the case of $P_{1.50}S_{1.00}$ does not follow the Meyer−Neldel rule (Figure 2). In this case, the ratio D_{Li^+}/D_{PEO} goes from below 1 to above 1 (Figure 3c), and the maximum D_{Li^+} value in the $S_{0.75}$ case is shifted toward lower ε_p and significantly larger than those in the case of $S_{1.00}$. All these observations point in the same direction: the Li-ion transport mechanisms are not the same when varying ε_p.

To investigate the Li$^+$ transport mechanism, the local solvation environment in the simulation box was tracked for the entire trajectories of the ions during the sampling time. The first maximum of the radial distribution function (RDF) between Li-O(PEO) was considered as the cutoff distance (see Supporting Information Section F, Figure S5). The indices of the PEO chains (1−200) within this cutoff distance were recorded every 200 ps, which is much shorter than the residence time of Li$^+$ (see Section E in the Supporting Information for details). Typical representative time evolutions of the Li$^+$ coordination to these PEO chain indices for systems with high, intermediate, and low solvent polarities are presented in Figure 4a,c,d for the $S_{1.00}$ case and in Figure 4b,d,f for the $S_{0.75}$ case for selected individual Li$^+$ ions in these different systems.

It can be seen from Figure 4a,b that at high ε_p, Li$^+$ ions typically stay with one or two PEO chains for more than 100 ns and then hop to another chain. This shows that the transport mechanism, in this case, was mainly intrachain diffusion, either as hopping between different oxygens on the same chain or as diffusion together with the polymer. At intermediate ε_p, where D_{Li^+} is maximum, the interchain hopping between different PEO molecules becomes much more frequent (Figure 4c,d). At low ε_p, the Li$^+$ ions seem to be barely coordinated to the PEO chains, which suggests they are instead mostly coordinated to TFSI ions (Figure 4e,f).

To confirm that the picture given by Figure 4a−f is indeed statistically significant, the probability of the number of PEO chains visited by Li$^+$ was calculated, and the corresponding distributions are presented in Figure 4g,h. It is seen that with an increase in solvent polarity, the average number of PEO chains visited by the individual Li$^+$ ions increase initially and then decreases at high ε_p. This is in accordance with Figure 4a−f and suggests a transition of the transport mechanism from a vehicular mechanism at low ε_p, to the frequent interchain hopping at intermediate ε_p, and to the intrachain hopping at high ε_p.

Previous studies[58,60−62] using a similar procedure have shown that the Li ions transported via interchain hopping
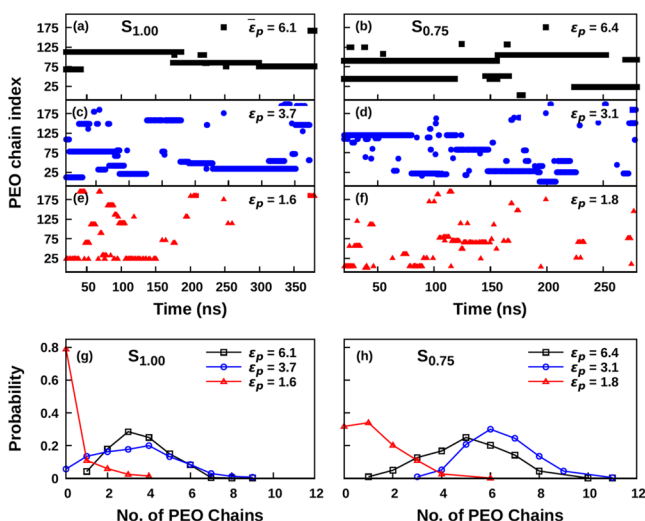
Figure 4. Li+-PEO chain coordination environments as a function of simulation time for the $S_{1.00}$ cases at ε_p = 6.1 (a), 3.7 (c), and 1.6 (e) and for the $S_{0.75}$ cases at ε_p = 6.4 (b), 3.1 (d), and 1.8 (f). The probability of the number of PEO chains visited by Li+ ion for the $S_{1.00}$ (g) and $S_{0.75}$ (h) cases. One visit is counted if Li+ stays with that PEO chain for more than 5% of simulation time (~20−30 ns).

Figure 5. Three-dimensional (3D) bar plot of D_{Li^+} as functions of coordination numbers (CNs) of Li+-O(PEO) (bottom left axis) and Li+-O(TFSI) (bottom right axis) at the normalized inverse temperature $1000/(T - T_g + 50)$ of 5.4 ($\pm$0.1). Representative snapshots of the first coordination shell of Li+ in different polarization environments are also shown. These snapshots show the crossover in Li+ coordination environment from TFSI to PEO with an increase in solvent polarity. Color coding of atoms: Li, violet; C, gray; N, blue; O, red; F, green; and S, yellow.

events have a higher diffusion coefficient than that from intrachain hopping or vehicular mechanisms. In fact, the vehicular mobility only corresponds to transport on a very short time scale, since the global macromolecular diffusivity at longer time scales is negligible, at least for higher molecular weights where the polymers are entangled. Consequently, this suggests that more frequent interchain hopping would lead to the highest diffusion coefficients, thereby justifying the maximum D_{Li^+} found in Figure 3a.

Previously, it has been shown that a further increase in polarity reduces the polymer segmental motion and leads to slow Li-ion diffusion.[17] This agrees with the observations in Figure 4a,b. However, characterizing the solvent polarity solely by ε_p should be treated with caution. As mentioned in the Introduction, charge scaling does not only modulate ε_p explicitly but also changes the bond polarity implicitly. Therefore, further analysis on the local Li-ion solvation environments during Li-on conduction is necessary to shed light on this issue.

3.4. Importance of the Local Solvation Environment on Li-Ion Conduction. The local solvation environment of Li+ in the system is studied from its coordination number (CN). The CN of oxygen atoms in TFS and in the PEO chains around Li+ can be calculated by integrating their RDFs, $g(r)$, to its first minimum (r_{min}), thereby only including the first coordination shell

$$CN_{Li^+-O(X)}(r_{min}) = 4\pi\rho \int_0^{r_{min}} g_{Li^+-O(X)}(r) r^2 \, dr \quad (4)$$

where ρ is the number density of oxygen atoms. The average number of O atoms around Li+ in the first coordination shell for all systems is 5.3 ($\pm$0.6). These observations are in good agreement with NDIS (neutron diffraction with isotopic substitution) experiments[63] and MD simulations[33,58,59] of similar systems.

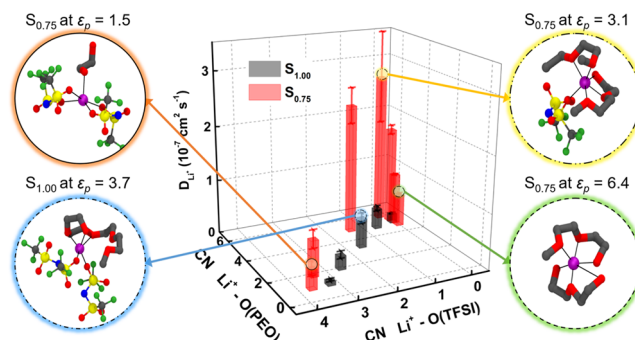The calculated CNs for Li+-O(PEO) and Li+-O(TFSI) in different polarization environments are plotted in Figure 5. At lower solvent polarity, Li+ is mostly coordinated by TFSI for both $S_{1.00}$ and $S_{0.75}$ cases (also see the snapshot on the top left side in Figure 5). This agrees with the 0.5 transference number found at low solvent polarity (Figure 3d), signaling that the ions have similar diffusivities and therefore are moving together. As the solvent polarity increases, there is a crossover in CNs of Li+-O(PEO) and Li+-O(TFSI) for both $S_{1.00}$ and $S_{0.75}$ (which were also illustrated in Figure 5). The CN of Li+-O(TFSI) is negligible at high solvent polarity, which indicates Li+ is mostly coordinated by the polymer matrix (the snapshot on the bottom right in Figure 5). To further illustrate the solvent environments, the fraction of contact ion pairs (CIPs) and the solvent separated ion pairs (SSIPs) were also calculated using cutoff distances from Li-O(TFSI) radial distribution functions (see Section F in the Supporting Information for details). From Figure S6, for both $S_{1.00}$ and $S_{0.75}$ cases, a crossover from CIPs to SSIPs can be observed at the solvent polarity where the maximum in D_{Li^+} is observed. This crossover point is in good agreement with the crossover point found for the CN of Li-O(PEO) and Li-O(TFSI).

What is important here is that the maximum D_{Li^+} shows up when the coordination of Li-ion involves both PEO and TFSI (the snapshot on the bottom left and top right in Figure 5). This suggests that an optimal solvating ability of polymer functional groups is crucial for fast Li-ion conduction in SPEs.

For systems having the maximum D_{Li^+}, it is found that TFSI facilitates the interchain hopping among the PEO chains. The Li+-PEO chain and Li+-TFSI coordination environments as a function of simulation time during the interchain hopping is given in Figure 6. In both $S_{1.00}$ and $S_{0.75}$ cases, the TFSI ions clearly get involved in the process. The TFSI ions thereby participate in forming good structural connectivity sites for ion hopping, which is necessary for fast ion conduction.[64] However, the Li+ is mostly coordinated to the same TFSI ions in the case of $S_{1.00}$ whereas it hops between different TFSI ions in the case of $S_{0.75}$. This difference may be attributed to the effect of electronic polarization through charge scaling of the salt.

4. CONCLUSIONS

In this work, the effect of the solvent polarity of PEO electrolytes on the Li+ diffusion has been investigated by
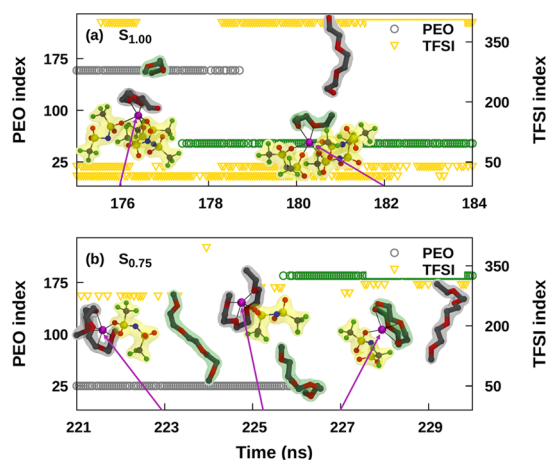
Figure 6. Li$^+$-PEO chain and Li$^+$-TFSI coordination environments as a function of simulation time during the interchain hopping (gray to green PEO chain) for the $S_{1.00}$ case at ε_p = 3.7 (a) and for the $S_{0.75}$ case at ε_p = 3.1 (b). Color coding of atoms: Li, violet; C, gray; N, blue; O, red; F, green; and S, yellow. Color coding of surfaces: PEO, gray and green, and TFSI, yellow.

employing charge scaling on PEO chains. All-atom MD simulations were carried to elucidate the coupling between local solvation environments and solvent polarity, which is out of reach for coarse-grained simulations. By comparing two cases where the point charges of LiTFSI are either intact or scaled down, both ionic and electronic screening effects of solvent were taken into account. It is found that the T_g of the PEO−LiTFSI system becomes higher with the increment of the solvent polarity as characterized by the dielectric constant of PEO, i.e., ε_p. The dependence of D_{Li^+} on the normalized temperature follows the so-called Meyer−Neldel rule in the low to intermediate range of ε_p.

By choosing a certain temperature normalized to T_g, the effect of T_g and the effect of solvent polarity were separated in our analysis. It was found that the maximum in the diffusion coefficient of Li$^+$ appears for intermediate values of ε_p. This is related to the fact that the ratio D_{Li+}/D_{PEO} goes from below 1 to above 1 with increasing ε_p. The corresponding transport mechanism changes from the vehicular mechanism, to the frequent interchain hopping, and then to the intrachain hopping. Since charge scaling does not only modulate ε_p explicitly but also implicitly tweaks the bond polarity (thereby the donor number), the maximum of D_{Li^+} can be rationalized by the optimal solvating ability of PEO at the intermediate value of ε_p. In particular, it was seen that balanced interactions between Li-ion with TSFI and PEO led to the frequent interchain hopping and the fast ion conduction.

These findings reveal the synergetic effect between solvent polarity and bond polarity for fast Li-ion diffusion in polymer electrolytes and provide insight for the rational design of the novel polymer electrolytes for solid-state Li-ion batteries.[65,66]

■ ASSOCIATED CONTENT

Ⓢ Supporting Information

The Supporting Information is available free of charge at https://pubs.acs.org/doi/10.1021/acs.jpcb.0c05108.

> Initial partial charges from the force field; equilibration checks for polymers in the system; determination of glass transition temperature (T_g), self-diffusion coef-

ficients from MSD, Li$^+$-O(PEO) residence time, radial distribution functions, and ion-pairing fractions (PDF)

■ AUTHOR INFORMATION

Corresponding Author

Chao Zhang − *Department of Chemistry—Ångström Laboratory, Uppsala University, 75121 Uppsala, Sweden;* ⓘ orcid.org/0000-0002-7167-0840; Email: chao.zhang@kemi.uu.se

Authors

Harish Gudla − *Department of Chemistry—Ångström Laboratory, Uppsala University, 75121 Uppsala, Sweden*

Daniel Brandell − *Department of Chemistry—Ångström Laboratory, Uppsala University, 75121 Uppsala, Sweden;* ⓘ orcid.org/0000-0002-8019-2801

Complete contact information is available at:
https://pubs.acs.org/10.1021/acs.jpcb.0c05108

Notes

The authors declare no competing financial interest.

■ REFERENCES

(1) Xue, Z.; He, D.; Xie, X. Poly(Ethylene Oxide)-Based Electrolytes for Lithium-Ion Batteries. *J. Mater. Chem. A* **2015**, *3*, 19218−19253.

(2) Li, Q.; Chen, J.; Fan, L.; Kong, X.; Lu, Y. Progress in Electrolytes for Rechargeable Li-Based Batteries and Beyond. *Green Energy Environ.* **2016**, *1*, 18−42.

(3) Teran, A. A.; Tang, M. H.; Mullin, S. A.; Balsara, N. P. Effect of Molecular Weight on Conductivity of Polymer Electrolytes. *Solid State Ionics* **2011**, *203*, 18−21.

(4) Devaux, D.; Bouchet, R.; Glé, D.; Denoyel, R. Mechanism of Ion Transport in PEO/LiTFSI Complexes: Effect of Temperature, Molecular Weight and End Groups. *Solid State Ionics* **2012**, *227*, 119−127.

(5) Timachova, K.; Watanabe, H.; Balsara, N. P. Effect of Molecular Weight and Salt Concentration on Ion Transport and the Transference Number in Polymer Electrolytes. *Macromolecules* **2015**, *48*, 7882−7888.

(6) Pożyczka, K.; Marzantowicz, M.; Dygas, J. R.; Krok, F. Ionic Conductivity and Lithium Transference Number of Poly(Ethylene Oxide):LiTFSI System. *Electrochim. Acta* **2017**, *227*, 127−135.

(7) Brandell, D.; Priimägi, P.; Kasemägi, H.; Aabloo, A. Branched Polyethylene/Poly(Ethylene Oxide) as a Host Matrix for Li-Ion Battery Electrolytes: A Molecular Dynamics Study. *Electrochim. Acta* **2011**, *57*, 228−236.

(8) Sengwa, R. J.; Kaur, K.; Chaudhary, R. Dielectric Properties of Low Molecular Weight Poly(Ethylene Glycol)s. *Polym. Int.* **2000**, *49*, 599−608.

(9) Karmakar, A.; Ghosh, A. Dielectric Permittivity and Electric Modulus of Polyethylene Oxide (PEO)-LiClO4 Composite Electrolytes. *Curr. Appl. Phys.* **2012**, *12*, 539−543.

(10) Kim, C. S.; Oh, S. M. Importance of Donor Number in Determining Solvating Ability of Polymers and Transport Properties in Gel-Type Polymer Electrolytes. *Electrochim. Acta* **2000**, *45*, 2101−2109.

(11) Ketkar, P. M.; Shen, K. H.; Hall, L. M.; Epps, T. H. Charging toward Improved Lithium-Ion Polymer Electrolytes: Exploiting Synergistic Experimental and Computational Approaches to Facilitate Materials Design. *Mol. Syst. Des. Eng.* **2019**, *4*, 223−238.

(12) Shen, K. H.; Hall, L. M. Ion Conductivity and Correlations in Model Salt-Doped Polymers: Effects of Interaction Strength and Concentration. *Macromolecules* **2020**, *10*, 58.

(13) Nakamura, I.; Wang, Z. G. Effects of Dielectric Inhomogeneity in Polyelectrolyte Solutions. *Soft Matter* **2013**, *9*, 5686−5690.

(14) Lin, K. J.; Maranas, J. K. Cation Coordination and Motion in a Poly(Ethylene Oxide)-Based Single Ion Conductor. *Macromolecules* **2012**, *45*, 6230−6240.

(15) Barteau, K. P. Poly(Glycidyl Ether)-Based Battery Electrolytes: Correlating Polymer Properties to Ion Transport. Ph.D. Thesis, University of California: Santa Barbara, CA, 2015.

(16) Wheatle, B. K.; Keith, J. R.; Mogurampelly, S.; Lynd, N. A.; Ganesan, V. Influence of Dielectric Constant on Ionic Transport in Polyether-Based Electrolytes. *ACS Macro Lett.* **2017**, *6*, 1362−1367.

(17) Wheatle, B. K.; Lynd, N. A.; Ganesan, V. Effect of Polymer Polarity on Ion Transport: A Competition between Ion Aggregation and Polymer Segmental Dynamics. *ACS Macro Lett.* **2018**, *7*, 1149−1154.

(18) Gutmann, V. Solvent Effects on the Reactivities of Organometallic Compounds. *Coord. Chem. Rev.* **1976**, *18*, 225−255.

(19) Schauser, N. S.; Grzetic, D. J.; Tabassum, T.; Kliegle, G. A.; Le, M. L.; Susca, E. M.; Antoine, S.; Keller, T. J.; Delaney, K. T.; Han, S.; et al. The Role of Backbone Polarity on Aggregation and Conduction of Ions in Polymer Electrolytes. *J. Am. Chem. Soc.* **2020**, *142*, 7055−7065.

(20) Borodin, O.; Smith, G. D. Development of Many-Body Polarizable Force Fields for Li-Battery Components: 1. Ether, Alkane, and Carbonate-Based Solvents. *J. Phys. Chem. B* **2006**, *110*, 6279−6292.

(21) Bedrov, D.; Piquemal, J. P.; Borodin, O.; MacKerell, A. D.; Roux, B.; Schröder, C. Molecular Dynamics Simulations of Ionic Liquids and Electrolytes Using Polarizable Force Fields. *Chem. Rev.* **2019**, *119*, 7940−7995.

(22) De Leeuw, S. W.; van Zon, A.; Bel, G. J. Structural Relaxation in Poly(Ethyleneoxide) and Poly(Ethyleneoxide)-Sodium Iodide Systems: A Molecular Dynamics Study. *Electrochim. Acta* **2001**, *46*, 1419−1426.

(23) Leontyev, I. V.; Stuchebrukhov, A. A. Electronic Continuum Model for Molecular Dynamics Simulations. *J. Chem. Phys.* **2009**, *130*, 85102−85109.

(24) Pegado, L.; Marsalek, O.; Jungwirth, P.; Wernersson, E. Solvation and Ion-Pairing Properties of the Aqueous Sulfate Anion: Explicit versus Effective Electronic Polarization. *Phys. Chem. Chem. Phys.* **2012**, *14*, 10210−10248.

(25) Kirby, B. J.; Pavel, J. Charge Scaling Manifesto: A Way of Reconciling the Inherently Macroscopic and Microscopic Natures of Molecular Simulations. *J. Phys. Chem. Lett.* **2019**, *10*, 7531−7536.

(26) Chen, X.; Chen, F.; Liu, M. S.; Forsyth, M. Polymer Architecture Effect on Sodium Ion Transport in PSTFSI-Based Ionomers: A Molecular Dynamics Study. *Solid State Ionics* **2016**, *288*, 271−276.

(27) Molinari, N.; Mailoa, J. P.; Kozinsky, B. Effect of Salt Concentration on Ion Clustering and Transport in Polymer Solid Electrolytes: A Molecular Dynamics Study of PEO−LiTFSI. *Chem. Mater.* **2018**, *30*, 6298−6306.

(28) Mogurampelly, S.; Ganesan, V. Structure and Mechanisms Underlying Ion Transport in Ternary Polymer Electrolytes Containing Ionic Liquids. *J. Chem. Phys.* **2017**, *146*, No. 074902.

(29) Costa, L. T.; Sun, B.; Jeschull, F.; Brandell, D. Polymer-Ionic Liquid Ternary Systems for Li-Battery Electrolytes: Molecular Dynamics Studies of LiTFSI in a EMIm-TFSI and PEO Blend. *J. Chem. Phys.* **2015**, *143*, No. 024904.

(30) Jorgensen, W. L.; Chandrasekhar, J.; Madura, J. D.; Impey, R. W.; Klein, M. L. Comparison of Simple Potential Functions for Simulating Liquid Water. *J. Chem. Phys.* **1983**, *79*, 926.

(31) Martínez, L.; Andrade, R.; Birgin, E. G.; Martínez, J. M. Packmol: A Package for Building Initial Configurations for Molecular Dynamics Simulations. *J. Comput. Chem.* **2009**, *30*, 2157−2164.

(32) Wang, J.; Wolf, R. M.; Caldwell, J. W.; Kollman, P. A.; Case, D. A. Development and Testing of a General Amber Force Field. *J. Comput. Chem.* **2004**, *25*, 1157−1174.

(33) Ebadi, M.; Costa, L. T.; Araujo, C. M.; Brandell, D. Modelling the Polymer Electrolyte/Li-Metal Interface by Molecular Dynamics Simulations. *Electrochim. Acta* **2017**, *234*, 43−51.

(34) Sprenger, K. G.; Jaeger, V. W.; Pfaendtner, J. The General AMBER Force Field (GAFF) Can Accurately Predict Thermodynamic and Transport Properties of Many Ionic Liquids. *J. Phys. Chem. B* **2015**, *119*, 5882−5895.

(35) Liu, H.; Paddison, S. J. Alkyl Chain Length Dependence of Backbone-to-Backbone Distance in Polymerized Ionic Liquids: An Atomistic Simulation Perspective on Scattering. *Macromolecules* **2017**, *50*, 2889−2895.

(36) Jakalian, A.; Jack, D. B.; Bayly, C. I. Fast, Efficient Generation of High-Quality Atomic Charges. AM1-BCC Model: II. Parameterization and Validation. *J. Comput. Chem.* **2002**, *23*, 1623−1641.

(37) Abraham, M. J.; van der Spoel, D.; Lindah, E.; Hess, B. *The GROMACS Development Team*, GROMACS User Manual version, 2018. http://www.gromacs.org.

(38) Abraham, M. J.; Murtola, T.; Schulz, R.; Páll, S.; Smith, J. C.; Hess, B.; Lindah, E. GROMACS: High Performance Molecular Simulations through Multi-Level Parallelism from Laptops to Supercomputers. *SoftwareX* **2015**, *1−2*, 19−25.

(39) Darden, T.; York, D.; Pedersen, L. Particle Mesh Ewald: An N·log(N) Method for Ewald Sums in Large Systems. *J. Chem. Phys.* **1993**, *98*, 10089−10092.

(40) Hess, B.; Bekker, H.; Berendsen, H. J. C.; Fraaije, J. G. E. M. LINCS: A Linear Constraint Solver for Molecular Simulations. *J. Comput. Chem.* **1997**, *18*, 1463−1472.

(41) Bussi, G.; Donadio, D.; Parrinello, M. Canonical Sampling through Velocity Rescaling. *J. Chem. Phys.* **2007**, *126*, No. 014101.

(42) Parrinello, M.; Rahman, A. Polymorphic Transitions in Single Crystals: A New Molecular Dynamics Method. *J. Appl. Phys.* **1981**, *52*, 7182−7190.

(43) Griffiths, T. R.; Pugh, D. C. Correlations among Solvent Polarity Scales, Dielectric Constant and Dipole Moment, and a Means to Reliable Predictions of Polarity Scale Values from Current Data. *Coord. Chem. Rev.* **1979**, *29*, 129−211.

(44) Neumann, M. Dipole Moment Fluctuation Formulas in Computer Simulations of Polar Systems. *Mol. Phys.* **1983**, *50*, 841−858.

(45) Aziz, S. B.; Abidin, Z. H. Z. Electrical Conduction Mechanism in Solid Polymer Electrolytes: New Concepts to Arrhenius Equation. *J. Soft Matter* **2013**, *2013*, 1−8.

(46) Aziz, S. B. Li+ Ion Conduction Mechanism in Poly (ε-Caprolactone)-Based Polymer Electrolyte. *Iran. Polym. J.* **2013**, *22*, 877−883.

(47) Hanke, E.; Von Roden, K.; Kaatze, U. Hydrogen Network Fluctuations of Associating Liquids: Dielectric Relaxation of Ethylene Glycol Oligomers and Their Mixtures with Water. *J. Chem. Phys.* **2006**, *125*, 84507.

(48) Kammer, H. W. Dielectric Relaxation in PEO-Based Polymer Electrolytes. *Ionics* **2018**, *24*, 1415−1428.

(49) Matsumiya, Y.; Balsara, N. P.; Kerr, J. B.; Inoue, T.; Watanabe, H. In Situ Dielectric Characterization of Poly(Ethylene Oxide) Melts Containing Lithium Perchlorate under Steady Shear Flow. *Macromolecules* **2004**, *37*, 544−553.

(50) Hayamizu, K.; Akiba, E.; Bando, T.; Aihara, Y. 1H, 7Li, and 19F Nuclear Magnetic Resonance and Ionic Conductivity Studies for Liquid Electrolytes Composed of Glymes and Polyethene glycol Dimethyl Ethers of CH3O(CH2CH2O)NCH3 (n = 3−50) Doped with LiN(SO2CF3)2. *J. Chem. Phys.* **2002**, *117*, 5929−5939.

(51) Wu, C. Simulated Glass Transition of Poly(Ethylene Oxide) Bulk and Film: A Comparative Study. *J. Phys. Chem. B* **2011**, *115*, 11044−11052.

(52) Lascaud, S.; Perrier, M.; Vallée, A.; Besner, S.; Prud'homme, J.; Armand, M. Phase Diagrams and Conductivity Behavior of Poly-(Ethylene Oxide)-Molten Salt Rubbery Electrolytes. *Macromolecules* **1994**, *27*, 7469−7477.

(53) Cameron, G. G.; Ingram, M. D.; Harvie, J. L. Ion Transport in Polymer Electrolytes. *Faraday Discuss. Chem. Soc.* **1989**, *88*, 55−63.

(54) Stolwijk, N. A.; Heddier, C.; Reschke, M.; Wiencierz, M.; Bokeloh, J.; Wilde, G. Salt-Concentration Dependence of the Glass Transition Temperature in PEO−NaI and PEO−LiTFSI Polymer Electrolytes. *Macromolecules* **2013**, *46*, 8580−8588.

(55) Zheng, Q.; Pesko, D. M.; Savoie, B. M.; Timachova, K.; Hasan, A. L.; Smith, M. C.; Miller, T. F.; Coates, G. W.; Balsara, N. P. Optimizing Ion Transport in Polyether-Based Electrolytes for Lithium Batteries. *Macromolecules* **2018**, *51*, 2847−2858.

(56) Maginn, E. J.; Messerly, R. A.; Carlson, D. J.; Roe, D. R.; Elliott, J. R. Best Practices for Computing Transport Properties 1. Self-Diffusivity and Viscosity from Equilibrium Molecular Dynamics [Article v1.0]. *Living J. Comput. Mol. Sci.* **2019**, *1*, 1−20.

(57) Dalvi, A.; Parvathala Reddy, N.; Agarwal, S. C. The Meyer−Neldel Rule and Hopping Conduction. *Solid State Commun.* **2012**, *152*, 612−615.

(58) Borodin, O.; Smith, G. D. Mechanism of Ion Transport in Amorphous Poly(Ethylene Oxide)/ LiTFSI from Molecular Dynamics Simulations. *Macromolecules* **2006**, *39*, 1620−1629.

(59) Brooks, D. J.; Merinov, B. V.; Goddard, W. A.; Kozinsky, B.; Mailoa, J. Atomistic Description of Ionic Diffusion in PEO−LiTFSI: Effect of Temperature, Molecular Weight, and Ionic Concentration. *Macromolecules* **2018**, *51*, 8987−8995.

(60) Müller-Plathe, F.; Van Gunsteren, W. F. Computer Simulation of a Polymer Electrolyte: Lithium Iodide in Amorphous Poly-(Ethylene Oxide). *J. Chem. Phys.* **1995**, *103*, 4745−4756.

(61) Borodin, O.; Smith, G. D.; Douglas, R. Force Field Development and MD Simulations of Poly(Ethylene Oxide)/LiBF4 Polymer Electrolytes. *J. Phys. Chem. B* **2003**, *107*, 6824−6837.

(62) Webb, M. A.; Jung, Y.; Pesko, D. M.; Savoie, B. M.; Yamamoto, U.; Coates, G. W.; Balsara, N. P.; Wang, Z. G.; Miller, T. F. Systematic Computational and Experimental Investigation of Lithium-Ion Transport Mechanisms in Polyester-Based Polymer Electrolytes. *ACS Cent. Sci.* **2015**, *1*, 198−205.

(63) Mao, G.; Saboungi, M.-L.; Price, D. L.; Armand, M. B.; Howells, W. S. Structure of Liquid PEO−LiTFSI Electrolyte. *Phys. Rev. Lett.* **2000**, *84*, 5536−5539.

(64) Ebadi, M.; Eriksson, T.; Mandal, P.; Costa, L. T.; Araujo, C. M.; Mindemark, J.; Brandell, D. Restricted Ion Transport by Plasticizing Side Chains in Polycarbonate-Based Solid Electrolytes. *Macromolecules* **2020**, *53*, 764−774.

(65) Mindemark, J.; Lacey, M. J.; Bowden, T.; Brandell, D. Beyond PEO—Alternative Host Materials for Li+-Conducting Solid Polymer Electrolytes. *Prog. Polym. Sci.* **2018**, *81*, 114−143.

(66) Barteau, K. P.; Wolffs, M.; Lynd, N. A.; Fredrickson, G. H.; Kramer, E. J.; Hawker, C. J. Allyl Glycidyl Ether-Based Polymer Electrolytes for Room Temperature Lithium Batteries. *Macromolecules* **2013**, *46*, 8988−8994.